



Article

Surface-Limited Electrodeposition of Continuous Platinum Networks on Highly Ordered Pyrolytic Graphite

Filippo Farina, Giorgio Ercolano, Sara Cavaliere * , Deborah J. Jones and Jacques Rozière

Institute Charles Gerhardt Montpellier, UMR CNRS 5253, Aggregates Interfaces and Materials for Energy, University of Montpellier, 34095 Montpellier CEDEX 5, France; filippo.farina@umontpellier.fr (F.F.); giorgio.ercolano@umontpellier.fr (G.E.); deborah.jones@umontpellier.fr (D.J.J.); jacques.roziere@umontpellier.fr (J.R.)

* Correspondence: sara.cavaliere@umontpellier.fr; Tel.: +33-467-149-098; Fax: +33-467-143-304

Received: 20 August 2018; Accepted: 11 September 2018; Published: 13 September 2018



Abstract: Continuous thin platinum nanoplatelet networks and thin films were obtained on the flat surface of highly ordered pyrolytic graphite (HOPG) by high overpotential electrodeposition. By increasing the deposition time, the morphology of the Pt deposits can be progressively tuned from isolated nanoplatelets, interconnected nanostructures, and thin large flat islands. The deposition is surface-limited and the thickness of the deposits, equivalent to 5 to 12 Pt monolayers, is not time dependent. The presence of Pt (111) facets is confirmed by High Resolution Transmission Electron Microscopy (HRTEM) and evidence for the early formation of a platinum monolayer is provided by Scanning Transmission Electron Microscopy and Energy Dispersive X-rays Spectroscopy (STEM-EDX) and X-ray Photoelectron Spectroscopy (XPS) analysis. The electroactivity towards the oxygen reduction reaction of the 2D deposits is also assessed, demonstrating their great potential in energy conversion devices where ultra-low loading of Pt via extended surfaces is a reliable strategy.

Keywords: electrodeposition; platinum; highly oriented pyrolytic graphite; 2D growth; thin films

1. Introduction

Carbon-supported platinum electrocatalysts are employed in the electrodes of Proton Exchange Membrane Fuel Cells (PEMFCs), but due to the scarcity of platinum and its cost [1], efforts to reduce the noble metal loading have driven research towards the development of strategies maximising its utilisation [2], including metal@platinum core@shell nanoparticles [3], platinum nanostructures [4] and thin films [5]. Several methods such as Atomic Layer Deposition (ALD) [6,7], Pulsed Laser Deposition (PLD) [8], Surface-Limited Redox Replacement (SLRR) [9], and Magnetron Sputtering (MS) [10] allow the preparation of extended Pt surfaces on various supports including carbon [11].

Electrodeposition of Pt in galvanostatic and potentiostatic modes is conventionally characterized by the 3D growth of platinum, which forms spherical, or flower-like, agglomerates [12–14]. Achieving the formation of thin Pt structures via electrodeposition therefore represents a real challenge. We recently observed that pulsed electrodeposition at high overpotentials can produce crystalline nanoplatelets on carbonaceous surfaces. Thin 2D Pt nanoplatelets were grown on electrospun carbon fibres and on nanotubes developed from their surfaces, and the resulting materials were evaluated as electrocatalysts for the Oxygen Reduction Reaction (ORR) in the cathode of a PEMFC, demonstrating enhanced exploitation of the noble metal [15,16]. Such nanofibres and nanotubes do not lend themselves to in-depth investigations using advanced microscopies, and so to further our understanding of this high overpotential electrodeposition method we turned our attention to

the model surface of Highly Ordered Pyrolytic Graphite (HOPG), and herein describe our findings. The aim is to investigate the process occurring on a flat carbon surface at the nanoscale, leading to the formation of crystalline nanoplatelets, interconnected nanostructures, and thin films. To achieve deposition with a single nucleation step, followed by increasing Pt growth for better insights into the deposit formation process, the electrodeposition approach developed in our previous work was modified to consider only a single potential pulse of varying duration. The choice of HOPG as a model surface is due to its relative flatness as well as to its structural similarity to the graphitized regions of the surface of the carbon nanofibers and nanotubes that inspired this work [15,16]. Furthermore, the possibility of exfoliating HOPG to obtain graphene layers [17], which can be further catalysed with platinum, will open novel perspectives of applications.

While studies of platinum electrodeposition on various carbonaceous surfaces have been reported [18–20], it appears that the process has been investigated mainly for slight overpotential conditions and not at the very high overpotentials (i.e. in the region of strong H₂ evolution) that are the conditions chosen here. It was previously reported that interconnected Pt structures can be obtained by applying an overpotential of -500 mV vs. SCE (-259 SHE) [21,22]. Such a high overpotential could in principle force two-dimensional growth in through underpotential deposition of hydrogen (H_{upd}) on the Pt surface, which prevents or impedes diffusion of the Pt precursor towards the surface of the newly electrodeposited Pt layers [23]. Spontaneous deposition of Pt agglomerates, nanoparticles, and networks on HOPG was induced from water as well as non-aqueous polar solvents [24–26] and was explained in terms of the reduction of Pt by oxidized defect sites on the surface and step-edges [24]. However, the mechanism appears to be more complex, involving not only graphite step-edges, but also hydrogenated sites [27,28]. As a consequence, Pt nuclei may be already present before the application of the overpotential to the electrode [28].

In this paper, we investigate the effect of a high overpotential single-pulse length on the morphology and crystal structure of the Pt deposits on the flat model carbon surface HOPG for better insights on the deposition mechanism and 2D growth of extended metal surfaces using microscopy and surface analysis techniques.

2. Materials and Methods

Highly Oriented Pyrolytic Graphite (HOPG, ZYH grade, 12 mm × 12 mm from Veeco-Bruker, Camarillo, CA, USA) was used as the working electrode in a two-electrode cell, and a 5 cm × 5 cm graphite sheet (Goodfellow) was used as the counter-shortened reference electrode (RE/CE). The working electrode assembly was masked with Kapton[®] tape (RS Components SAS, Beauvais, France), leaving a 6 mm × 6 mm HOPG surface exposed to the precursor solution, and the HOPG back-plate was connected with a platinum wire to the potentiostat (Bio-Logic[®] SP300, Bio-Logic SAS, Seyssinet-Pariset, France). Electrodeposition experiments were performed at -3 V vs. RE/CE (measured to be equivalent in the same cell geometry to -1.9 V vs. Ag/AgCl) for various duration times (from 5 to 200 s), followed by 60 s at open circuit voltage (OCV). The deposition solution was a solution of 3 mM hexachloroplatinic acid hexahydrate ($\geq 99.9\%$ trace metal basis) and 0.5 M sodium chloride in MilliQ water (18 M Ω cm). All chemicals were provided by Sigma-Aldrich, St. Louis, MO, USA. An iR correction was performed before each electrodeposition step with the typical electrical resistance being in the range 10–20 Ω ; the distance between the electrodes was fixed at 5 cm. Before electrodeposition, the solution was cooled to ~ 4 °C in an ice bath and purged with nitrogen to remove the dissolved oxygen. During the deposition, the precursor solution was stirred at 900 rpm to remove the hydrogen bubbles that evolve on the surface of the HOPG and to limit the thickness of the precursor diffusion layer. Prior to any characterization, the deposited sample was thoroughly rinsed with MilliQ grade water. Tapping Mode Atomic Force Microscopy (TM-AFM) images were acquired with a Bruker Nanoman (Bruker SAS, Palaiseau, France) driven by Nanoscope 5 electronics. The cantilever tips were Silicon Point Probe Plus[®] NCSTR (Nanosensors, Neuchâtel, Switzerland; force constant 6.5 N/m, resonance frequency 157 kHz). All the image treatments and the thickness measurements were performed using WSxM 4.0

Beta 8.2 [29] and the resulting data were treated with the Fityk software [30] to correct the background. Particle size measurements and Fast Fourier Transforms were performed with ImageJ 1.48 v (U. S. National Institutes of Health, Bethesda, MD, USA). High Resolution Transmission Electron Microscopy (HRTEM), Scanning Transmission Electron Microscopy (STEM) micrographs and Energy Dispersive X-rays Spectroscopy (EDX) data were obtained with a JEOL 2200FS (Source: FEG) microscope (JEOL Europe SAS, Croissy-sur-Seine, France) operating at 200 kV and equipped with a CCD camera Gatan USC (16 MP; Gatan, Evry, France). The samples were prepared by carefully peeling away flakes of HOPG and depositing them onto a Cu grid with a drop of silver paste. Scanning electron micrographs were acquired by Field Emission-Scanning Electron Microscopy (FE-SEM) using a Hitachi S-4800 microscope (Hitachi Europe SAS, Velizy, France). The surface composition of the samples was investigated by X-ray Photoelectron Spectroscopy (XPS) on an ESCALAB 250 (Thermo Electron, Villebon Sur Yvette, France). The X-ray excitation was provided by a monochromatic Al K_{α} (1486.6 eV) source, and the analysed surface area was 400 μm^2 . A constant analyser energy mode was used for the electron detection (20 eV pass energy). Detection of the emitted photoelectrons was performed perpendicular to the surface sample. Data quantification was performed on the Avantage software (Thermo Fisher Scientific, Waltham, MA, USA), removing the background signal using the Shirley method. The surface atomic concentrations were determined from photoelectron peaks areas using the atomic sensitivity factors reported by Scofield. Binding energies of all core levels are referenced to the C–C bond of C 1s (284.8 eV). Linear sweep voltammetry (LSV) was performed at 20 mV s^{-1} in O_2 saturated 0.1 M HClO_4 on a Bio-Logic[®] SP300 potentiostat (see above); the working electrode was an HOPG-Pt sample connected to the potentiostat with a Pt wire, while the counter electrode was a graphite rod (Alfa Aesar, Heysam, UK) and reference used was an Ag/AgCl electrode (Fisher Scientific, Illkirch, France; $E = 0.197 \text{ V vs. NHE}$). The potentials in the manuscript were reported vs. NHE.

3. Results and Discussion

3.1. TM-AFM Analysis

Tapping Mode Atomic Force Microscopy (TM-AFM) images of electrodeposited Pt samples prepared with different pulse durations are shown in Figure 1, together with their thickness and diameter distributions.

Only separate Pt nanoplatelets were visible for a 5 s deposition time, while thin Pt networks started to clearly form after a 10 s deposition, and progressively covered the surface of the HOPG substrate up to 40 s and, at 200 s, thin large flat Pt islands were fully formed. Larger agglomerates of Pt were also present along all the samples, whatever the pulse duration, possibly formed either during the open circuit voltage (OCV) step of the electrodeposition process or as a result of H_2 -induced precipitation [23]. The Pt morphologies resulting from the application of this overpotential method in the range 5–40 s appear to be partially similar to previous reports, but they clearly show that the substrate surface is progressive covered with a network of interconnected flat Pt nanostructures of low thickness [21,22]. An increase of the degree of interconnection of the Pt nanoplatelets is clearly visible with an increase in deposition time. A general trend can be derived for the sample series, however one might take into account a certain intra-sample inhomogeneity.

As shown in Figure 2a and Table 1, the thickness of the Pt nanoplatelets only slightly changed with deposition time. Most of the nanoplatelets did not grow over 4 nm in thickness even at longer deposition times (Table 1), with the average being comprised between 1.0 and 2.5 nm (equivalent to 5 to 12 Pt monolayers). Pt deposits with comparable thickness and diameter were reported for slight overpotential conditions and shorter times as well, but there was no evidence of interconnected or extended surface structures [31].

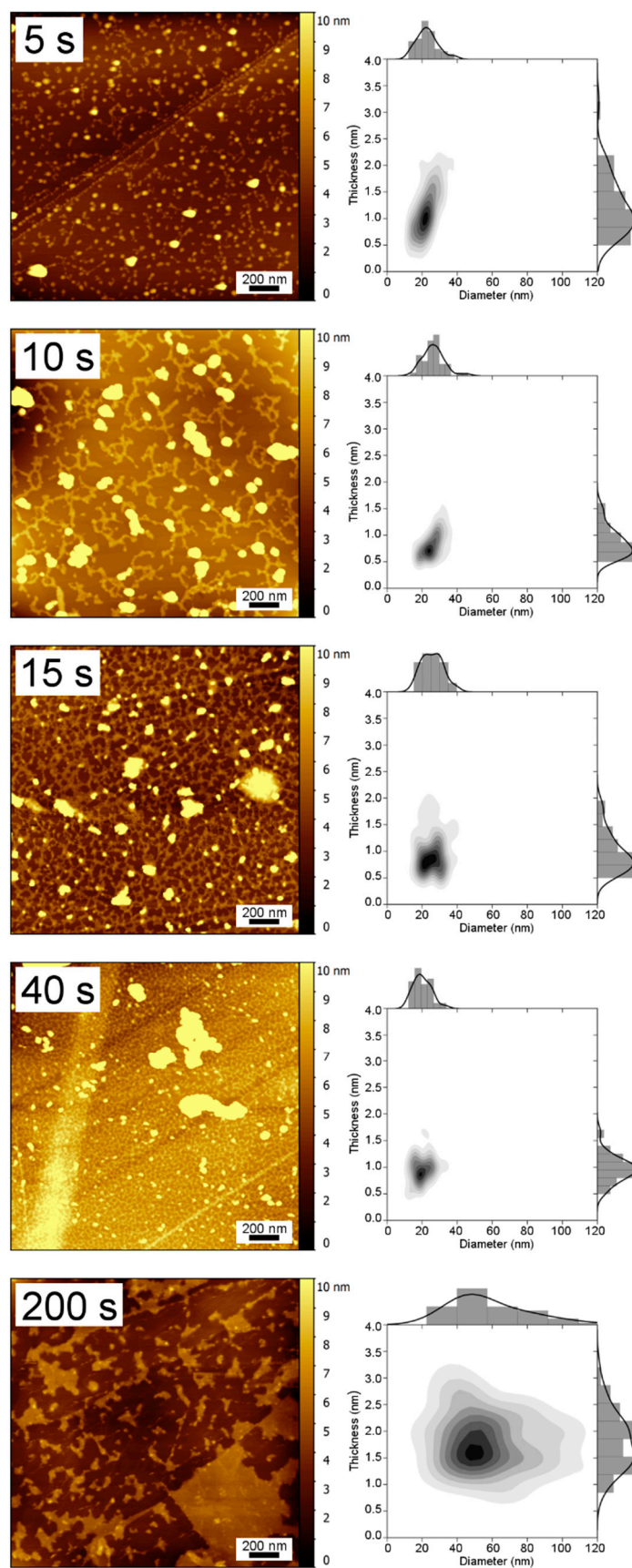


Figure 1. TM-AFM images of Pt on HOPG electrodeposited at different pulse times (left, scale bars are 200 nm) with the respective thickness and diameter bivariate distributions (right).

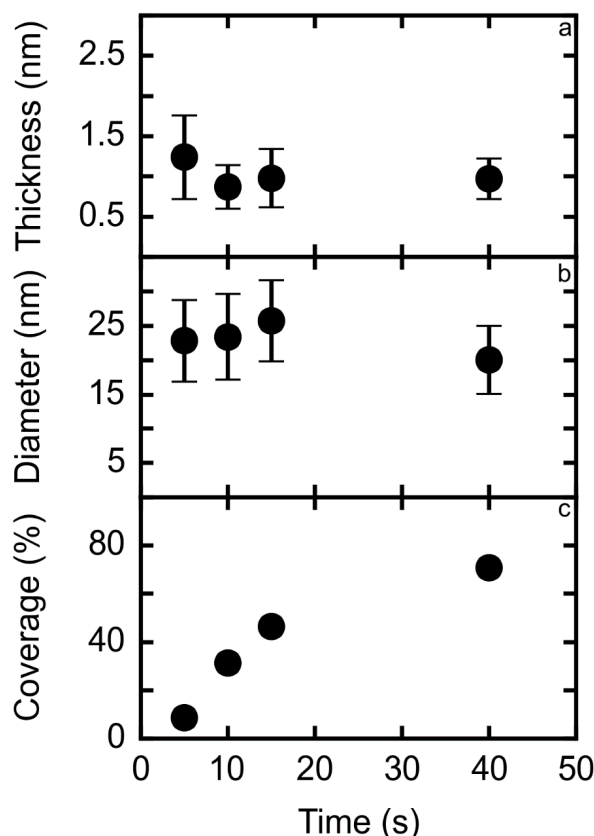


Figure 2. Dependence of average Pt nanoplatelets thickness (with standard deviation) (a) average Pt nanoplatelets diameter (with standard deviation). (b) and percentage of covered surface. (c) on the deposition time. The sample obtained with a 200 s pulse is not included for clarity (see Table 1).

Table 1. Dependence of average thickness and diameter of the electrodeposited Pt nanoplatelets on the deposition time. Surface coverage percentage was calculated on the AFM micrographs shown in Figure 1.

Sample	Thickness (nm)	Diameter (nm)	Surface Coverage (%)
5	1.24 ± 0.52	22.8 ± 6	8.7
10	0.87 ± 0.27	23.4 ± 6	31.4
15	0.98 ± 0.36	25.8 ± 6	46.5
40	0.97 ± 0.25	20.1 ± 5	70.7
200	1.82 ± 0.52	72.0 ± 69	44.9

Similarly, the average nanoplatelet diameter did not vary greatly with the deposition time (Figure 2b) and the size distribution is reasonably similar for all the samples (Figure 1). Although the diameter of the platinum islands is comparable to some reported for other overpotential conditions [32], the present high overpotential conditions lead to a distinct geometry in that the diameter is roughly 20 times the thickness for samples in the 5–40 s time interval, confirming the presence of flat nanoplatelets and thus two-dimensional growth.

The percentage of surface coverage increases with the deposition time (Figure 2c), indicating a surface-limited electrodeposition in the range 5–40 s. The sample prepared with 200 s deposition duration presented different values both for size distribution and dimension ratio due to its clear film-like morphology, dissimilar to the interconnected networks observed at shorter deposition times. It should be noticed that the obtained morphologies and trends are reproducible, while the current densities obtained for Pt electrodeposition can be slightly different from one sample to another. This is due to the different conditions of the HOPG surface exposed by cleavage of the C–C stacking [28].

Different overpotential conditions may affect the aspect of the resulting Pt deposit, and phenomena such as secondary nucleation, surface diffusion, and coalescence should be taken into account to explain the formation of the different structures and morphologies [32]. The supporting electrolyte also takes part in the Pt growth mechanism and in determining the final morphology of the resulting deposit [22,33], its role depending on the concentration, and on the applied potential. In this work, a chloride supporting electrolyte was chosen for compatibility with the Pt precursor (H_2PtCl_6) possibly releasing the same anion. The 0.5 M NaCl solution provided a high concentration of Cl^- anions that may adsorb on the surface of the newly formed Pt structures, preventing further Pt atoms from depositing and growing in a three dimensional way [21,33]. Simultaneous adsorption of H and Cl species on Pt could also occur, possibly synergistically [34,35], or competitively, with the possibility also that at high overpotential only protons are adsorbed [36]. Adsorbed anions may also be partially responsible for the smaller Pt particles migrating from one active site to another or to other Pt surfaces [22,37]. This phenomenon may represent a possible or at least partial explanation for the presence of large Pt agglomerates in these samples. In the very high overpotential conditions used in this work, it is likely that no Cl^- is adsorbed on the Pt surfaces, due to the strong evolution of gaseous H_2 . The substrate also plays a role in Pt growth. Indeed, spontaneous electroless deposition on HOPG has been observed from Pt solutions, indicating the presence of metal seeds before the overpotential electrodeposition. The reducing agents for this spontaneous deposition are likely HOPG step edges that get oxidized in solution [28].

3.2. Electron Microscopy Analysis

High resolution transmission electron microscopy (HRTEM) micrographs of a Pt on an HOPG sample electrodeposited using a 15 s pulse were acquired to confirm the chemical nature and morphology of the deposit (Figure 3). The dimensions of the nanoplatelets were around 10 nm. The Fast Fourier Transform (FFT) analysis on selected areas of the TEM image, shown in Figure 3, presents three regions denoted A, B, and C with different d-spacings for the regions where carbon (A) and platinum (B) were clearly distinguishable.

In region A, only a single maximum at 0.21 nm is observed, comparable with the d-spacing of the (011) plane of graphite (0.2031 nm in JCPDS 96-901-2231). Region B clearly corresponds to a Pt platelet with a marked contrast over the carbon background. Indeed, in this region, a d-spacing of 0.23 nm was measured, fully compatible with that of the (111) facet of Pt (0.2299 nm in JCPDS 96-151-2257). In region C, no clear contrast nor evidence for platinum is visible from the TEM image. However, the FFT displays 3 maxima (one of 0.21 nm and two of 0.23 nm) demonstrating the presence of an extremely thin platinum layer, which was further corroborated by use of other techniques. Thus, to seek further evidence for the presence of Pt layers in areas where no obvious contrast was visible by imaging only, Energy Dispersive X-ray Spectroscopy (EDX) spectra on a Scanning Transmission Electron Microscopy (STEM) micrograph were recorded. Similarly to a previous report [38], local elemental analysis was performed on three different morphological features (Pt aggregate, Pt nanoplatelet and apparently bare HOPG) situated in another area of the same sample of Figure 3. The EDX spectra of the three zones highlighted in Figure 4 unquestionably show a Pt signal (Figure 4, inset) also in areas where no Pt nanoplatelets are visible by STEM. To conclude, the electron microscopy results depicted in Figures 3 and 4 provide complementary evidence for the presence of electrodeposited Pt all over the HOPG surface, demonstrating the early stage formation of a continuous ultra-thin electrodeposited Pt layer.

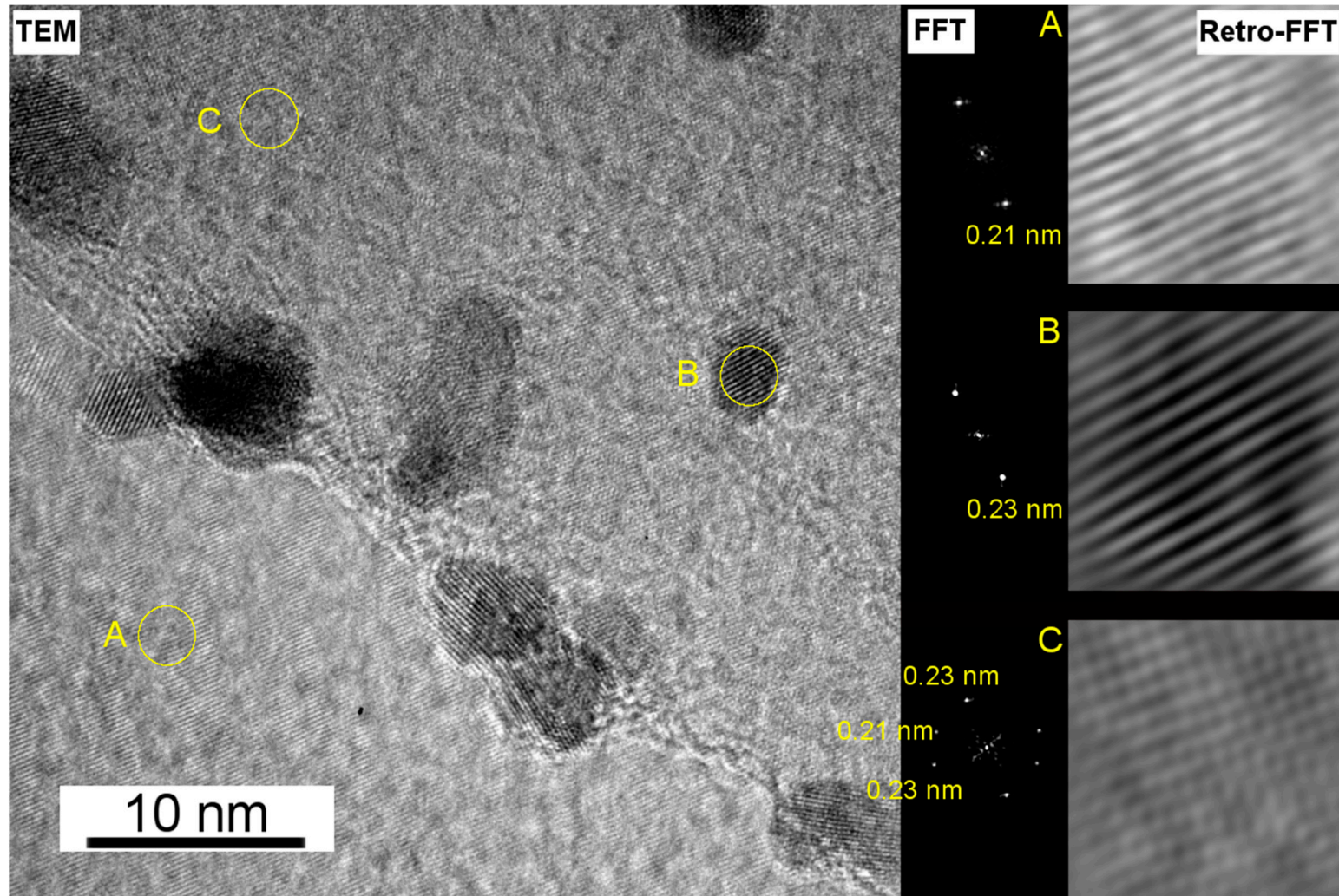


Figure 3. HRTEM micrograph of a slice of HOPG decorated with Pt nanoplatelets (**left**). FFT images of the three selected areas (**centre**) and the derived inverse-FFT (**right**).

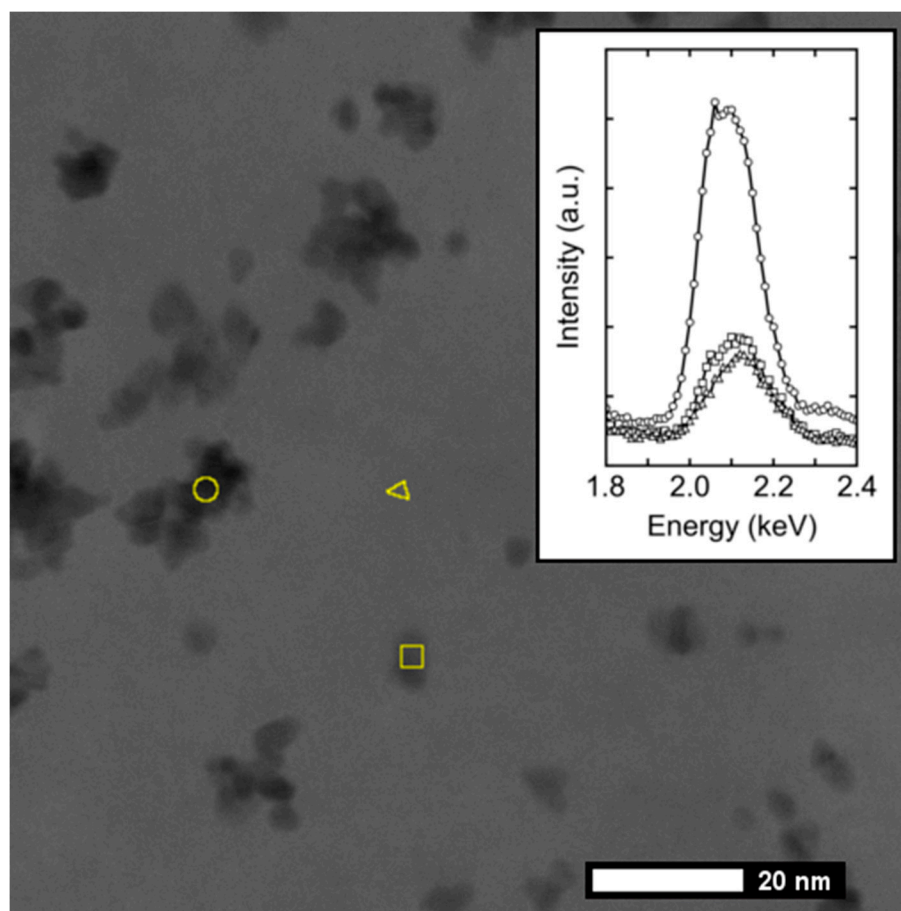


Figure 4. STEM micrograph of a flake of HOPG decorated with Pt aggregates (○) and Pt nanoplalelets (□); the comparison of their EDX spectra with the apparent bare surface of HOPG (Δ) is reported in the inset.

3.3. XPS Characterization

Surface analysis by X-ray Photoelectron Spectroscopy (XPS) was performed on a sample electrodeposited for 200 s both to further endorse the deposition of platinum, as well as to determine its oxidation state (Figure 5). The A bands of the Pt doublet observed on the sample (Pt 4f_{7/2} at 71.3 eV, Pt 4f_{5/2} at 74.6 eV) correspond to metallic Pt deposited on the HOPG surface. Additional contributions of B bands (72.2 and 75.5 eV respectively) were detected and related to the presence of oxidized forms of Pt, such as PtO_{ads} and/or Pt(OH)₂ [39]. The deconvolution of the Pt 4f doublet peaks indicates that Pt⁰ is the majority species (73.6% of the total signal, comparable to Pt freshly electrodeposited onto graphite substrates previously reported [40]), rather than ionic Pt, which confirms the predominant metallic nature of the deposit and thus the suitability of the technique to prepare catalytically active Pt thin films.

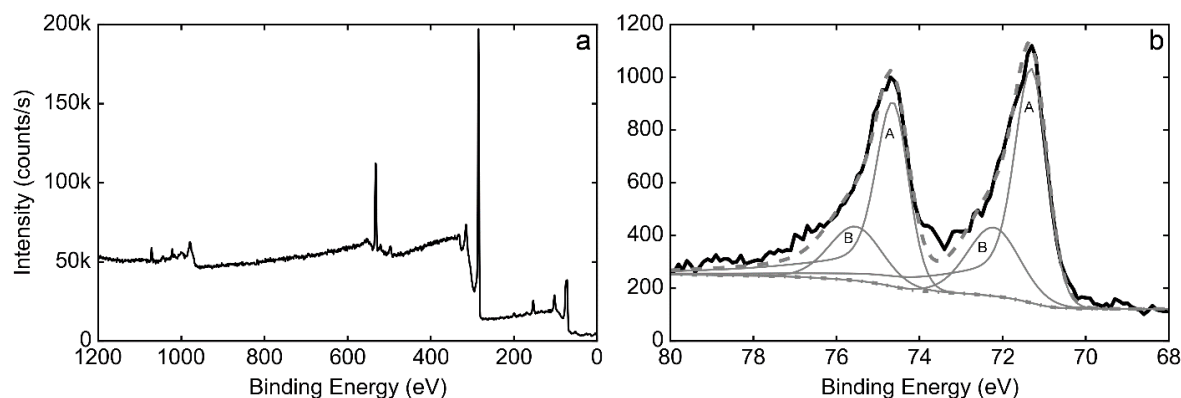


Figure 5. Survey XPS spectrum of a HOPG-Pt sample deposited for 200 s (a) and high-resolution spectrum of the Pt 4f region with peaks deconvolution (b).

The resulting Pt 4f spectrum is consistent with those reported for Pt films on HOPG with different thicknesses prepared by sputtering [41,42]. It is known that a Pt film thicker than 0.1 Å can already produce an XPS profile with two differentiated peaks, and since the sample prepared in this work also presented some Pt aggregates, the spectrum is the result of the presence of both 2D and 3D structures.

3.4. Electrocatalytic Activity

To assess the catalytic properties of the electrodeposited metal towards the oxygen reduction reaction (ORR), an HOPG-Pt sample deposited for 200 s was analyzed in O₂ saturated 0.1 M HClO₄ in a classical three-electrode configuration (scan from 1.2 to 0.3 V vs. NHE). The linear sweep voltammetry (LSV) shown in Figure 6 demonstrates that the deposited Pt⁰ is active, with an onset potential of ca 0.98 V vs. NHE. No reliable mass activity values could be derived due to the experimental conditions that are far from steady-state.

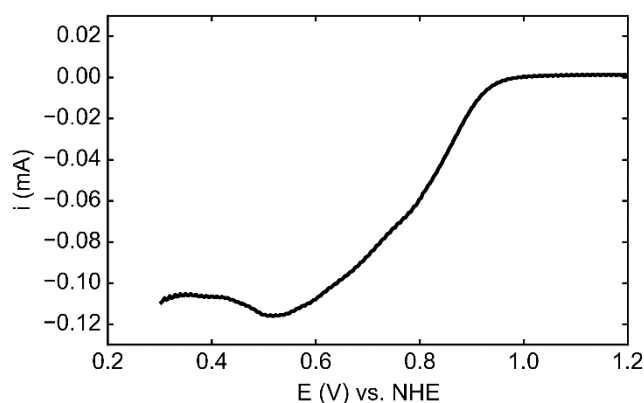


Figure 6. LSV of a HOPG-Pt sample electrodeposited for 200 s in O₂ saturated 0.1 M HClO₄ at 20 mV s⁻¹.

4. Conclusions

In conclusion, Pt nanoplatelet networks and Pt thin films were deposited on HOPG by high overpotential electrodeposition with a morphology that depends on pulse duration. The Pt networks formed using 5–40 s pulses comprised of extended islands of average thickness of 1 nm that were fairly homogeneous in diameter (20 times the thickness). Ultra-thin (<2 nm) Pt films are formed at a longer pulse time, 200 s, in which the exposed surfaces are Pt (111) facets. HR-TEM and XPS analysis confirm the metallic nature of the platinum deposit. These greater insights on the morphology of Pt structures deposited at high overpotential could only be obtained on a model carbon surface such as HOPG and will now serve to achieve complete formation of conformal and continuous ultra-thin Pt films on other

carbonaceous surfaces (e.g., nanofibers, nanotubes, etc . . .) of applicability in energy conversion, such as the development of ultra-low platinum loaded fuel cell electrodes.

Author Contributions: Conceptualization, S.C., D.J.J. and J.R.; Methodology, G.E., S.C., D.J.J. and J.R.; Formal Analysis, F.F., G.E.; Investigation, F.F., G.E.; Resources, S.C., D.J.J. and J.R.; Writing-Original Draft Preparation, F.F.; Writing-Review & Editing, G.E., S.C., D.J.J. and J.R.; Supervision, S.C., D.J.J. and J.R.; Project Administration, S.C.; Funding Acquisition, S.C.

Funding: The research leading to these results has received funding from the European Research Council (ERC) under the European Union's Seventh Framework Programme (FP/2007-2013)/ERC Grant Agreement SPINAM n. 306682. SC also acknowledges the support of the French IUF.

Acknowledgments: Michel Ramonda (Centrale de Technologie en Micro et nanoélectronique, CTM, University of Montpellier) is acknowledged for AFM image acquisition and helpful discussions.

Conflicts of Interest: The authors declare no conflict of interest.

References

1. Guerrero Moreno, N.; Cisneros Molina, M.; Gervasio, D.; Pérez Robles, J.F. Approaches to polymer electrolyte membrane fuel cells (PEMFCs) and their cost. *Renew. Sustain. Energy Rev.* **2015**, *52*, 897–906. [[CrossRef](#)]
2. Ercolano, G.; Cavaliere, S.; Rozière, J.; Jones, D.J. Recent developments in electrocatalyst design thriving noble metals in fuel cells. *Curr. Opin. Electrochem.* **2018**, *9*, 271–277. [[CrossRef](#)]
3. Gan, L.; Heggen, M.; Rudi, S.; Strasser, P. Core–shell compositional fine structures of dealloyed Pt. *Nano Lett.* **2012**, *12*, 5423–5430. [[CrossRef](#)] [[PubMed](#)]
4. Zhu, C.; Du, D.; Eychmüller, A.; Lin, Y. Engineering ordered and nonordered porous noble metal nanostructures: Synthesis, assembly, and their applications in electrochemistry. *Chem. Rev.* **2015**, *115*, 8896–8943. [[CrossRef](#)] [[PubMed](#)]
5. Cho, K.Y.; Yeom, Y.S.; Seo, H.Y.; Kumar, P.; Baek, K.-Y.; Yoon, H.G. A facile synthetic route for highly durable mesoporous platinum thin film electrocatalysts based on graphene: morphological and support effects on the oxygen reduction reaction. *J. Mater. Chem. A* **2017**, *5*, 3129–3135. [[CrossRef](#)]
6. Lee, H.B.R.; Baeck, S.H.; Jaramillo, T.F.; Bent, S.F. Growth of Pt nanowires by atomic layer deposition on highly ordered pyrolytic graphite. *Nano Lett.* **2013**, *13*, 457–463. [[CrossRef](#)] [[PubMed](#)]
7. Aaltonen, T.; Ritala, M.; Sajavaara, T.; Keinonen, J.; Leskelä, M. Atomic layer deposition of platinum thin films. *Chem. Mater.* **2003**, *15*, 1924–1928. [[CrossRef](#)]
8. Dolbec, R.; El Khakani, M.A. Sub-ppm sensitivity towards carbon monoxide by means of pulsed laser deposited SnO₂:Pt based sensors. *Appl. Phys. Lett.* **2007**, *90*, 173114. [[CrossRef](#)]
9. Achari, I.; Ambrozik, S.; Dimitrov, N. Electrochemical atomic layer deposition of Pd ultrathin films by surface limited redox replacement of underpotentially deposited H in a single cell. *J. Phys. Chem. C* **2017**, *121*, 4404–4411. [[CrossRef](#)]
10. Gruber, D.; Ponath, N.; Müller, J.; Lindstaedt, F. Sputter-deposited ultra-low catalyst loadings for PEM fuel cells. *J. Power Sources* **2005**, *150*, 67–72. [[CrossRef](#)]
11. Su, X.; Zhan, X.; Hinds, B.J. Pt monolayer deposition onto carbon nanotube mattes with high electrochemical activity. *J. Mater. Chem.* **2012**, *22*, 7979. [[CrossRef](#)]
12. Whalen, J.J.; Weiland, J.D.; Searson, P.C. Electrochemical deposition of platinum from aqueous ammonium hexachloroplatinate solution. *J. Electrochem. Soc.* **2005**, *152*, C738. [[CrossRef](#)]
13. Chen, X.; Li, N.; Eckhard, K.; Stoica, L.; Xia, W.; Assmann, J.; Muhler, M.; Schuhmann, W. Pulsed electrodeposition of Pt nanoclusters on carbon nanotubes modified carbon materials using diffusion restricting viscous electrolytes. *Electrochem. Commun.* **2007**, *9*, 1348–1354. [[CrossRef](#)]
14. Ye, F.; Chen, L.; Li, J.; Li, J.; Wang, X. Shape-controlled fabrication of platinum electrocatalyst by pulse electrodeposition. *Electrochem. Commun.* **2008**, *10*, 476–479. [[CrossRef](#)]
15. Ercolano, G.; Farina, F.; Cavaliere, S.; Jones, D.J.; Rozière, J. Towards ultrathin Pt films on nanofibres by surface-limited electrodeposition for electrocatalytic applications. *J. Mater. Chem. A* **2017**, *5*, 3974–3980. [[CrossRef](#)]
16. Ercolano, G.; Farina, F.; Cavaliere, S.; Jones, D.J.; Rozière, J. Multilayer hierarchical nanofibrillar electrodes with tuneable lacunarity with 2D like Pt deposits for PEMFC. *ECS Trans.* **2017**, *80*, 757–762. [[CrossRef](#)]

17. Yivlialin, R.; Bussetti, G.; Brambilla, L.; Castiglioni, C.; Tommasini, M.; Duò, L.; Passoni, M.; Ghidelli, M.; Casari, C.S.; Li Bassi, A. Microscopic analysis of the different perchlorate anions intercalation stages of graphite. *J. Phys. Chem. C* **2017**, *121*, 14246–14253. [[CrossRef](#)]
18. Yasin, H.M.; Denuault, G.; Pletcher, D. Studies of the electrodeposition of platinum metal from a hexachloroplatinic acid bath. *J. Electroanal. Chem.* **2009**, *633*, 327–332. [[CrossRef](#)]
19. Pang, L.; Zhang, Y.; Liu, S. Monolayer-by-monolayer growth of platinum films on complex carbon fiber paper structure. *Appl. Surf. Sci.* **2017**, *407*, 386–390. [[CrossRef](#)]
20. Duarte, M.M.E.; Pilla, A.S.; Sieben, J.M.; Mayer, C.E. Platinum particles electrodeposition on carbon substrates. *Electrochem. Commun.* **2006**, *8*, 159–164. [[CrossRef](#)]
21. Lee, I.; Chan, K.-Y.; Lee Phillips, D. Atomic force microscopy of platinum nanoparticles prepared on highly oriented pyrolytic graphite. *Ultramicroscopy* **1998**, *75*, 69–76. [[CrossRef](#)]
22. Lee, I.; Chan, K.-Y.; Phillips, D.L. Growth of electrodeposited platinum nanocrystals studied by atomic force microscopy. *Appl. Surf. Sci.* **1998**, *136*, 321–330. [[CrossRef](#)]
23. Liu, Y.H.; Gokcen, D.; Bertocci, U.; Moffat, T.P. Self-terminating growth of platinum films by electrochemical deposition. *Science* **2012**, *338*, 1327–1330. [[CrossRef](#)] [[PubMed](#)]
24. Zoval, J.V.; Lee, J.; Gorer, S.; Penner, R.M. Electrochemical preparation of platinum nanocrystallites with size selectivity on basal plane oriented graphite surfaces. *J. Phys. Chem. B* **1998**, *5647*, 1166–1175. [[CrossRef](#)]
25. Shen, P.; Chi, N.; Chan, K.Y.; Phillips, D.L. Platinum nanoparticles spontaneously formed on HOPG. *Appl. Surf. Sci.* **2001**, *172*, 159–166. [[CrossRef](#)]
26. Arroyo Gómez, J.J.; García, S.G. Spontaneous deposition of Pt-nanoparticles on HOPG surfaces. *Surf. Interface Anal.* **2015**, *47*, 1127–1131. [[CrossRef](#)]
27. Juarez, M.F.; Fuentes, S.; Soldano, G.J.; Avalle, L.; Santos, E. Spontaneous formation of metallic nanostructures on highly oriented pyrolytic graphite (HOPG): An ab initio and experimental study. *Faraday Discuss.* **2014**, *172*, 327–347. [[CrossRef](#)] [[PubMed](#)]
28. Alpuche-Aviles, M.A.; Farina, F.; Ercolano, G.; Subedi, P.; Cavaliere, S.; Jones, D.J.; Rozière, J. Electrodeposition of two-dimensional Pt nanostructures on highly oriented pyrolytic graphite (HOPG): the effect of evolved hydrogen and chloride ions. *Nanomaterials* **2018**, *8*, 668. [[CrossRef](#)]
29. Horcas, I.; Fernández, R.; Gómez-Rodríguez, J.M.; Colchero, J.; Gómez-Herrero, J.; Baro, A.M. WSXM: A software for scanning probe microscopy and a tool for nanotechnology. *Rev. Sci. Instrum.* **2007**, *78*. [[CrossRef](#)] [[PubMed](#)]
30. Wojdyr, M. Fityk: A general-purpose peak fitting program. *J. Appl. Crystallogr.* **2010**, *43*, 1126–1128. [[CrossRef](#)]
31. Lu, G.; Zangari, G. Electrodeposition of platinum nanoparticles on highly oriented pyrolytic graphite: Part II: Morphological characterization by atomic force microscopy. *Electrochim. Acta* **2006**, *51*, 2531–2538. [[CrossRef](#)]
32. Ustarroz, J.; Altantzis, T.; Hammons, J.A.; Hubin, A.; Bals, S.; Terry, H. The role of nanocluster aggregation, coalescence, and recrystallization in the electrochemical deposition of platinum nanostructures. *Chem. Mater.* **2014**, *26*, 2396–2406. [[CrossRef](#)]
33. Lu, G.J.; Zangari, G. Electrodeposition of platinum on highly oriented pyrolytic graphite. Part 1: Electrochemical characterization. *J. Phys. Chem. B* **2005**, *109*, 7998–8007. [[CrossRef](#)] [[PubMed](#)]
34. Li, N.; Lipkowsky, J. Chronocoulometric studies of chloride adsorption at the Pt(111) electrode surface. *J. Electroanal. Chem.* **2000**, *491*, 95–102. [[CrossRef](#)]
35. Horanyi, G.; Rizmayer, E.Z. A coupled voltammetric and radiometric (voltradiometric) study of the simultaneous adsorption of hydrogen and anions at platinized platinum electrodes. *J. Electroanal. Chem.* **1987**, *218*, 337–340. [[CrossRef](#)]
36. Gossenberger, F.; Roman, T.; Groß, A. Hydrogen and halide co-adsorption on Pt(111) in an electrochemical environment: A computational perspective. *Electrochim. Acta* **2016**, *216*, 152–159. [[CrossRef](#)]
37. Zhang, Z.C.; Beard, B.C. Agglomeration of Pt particles in the presence of chlorides. *Appl. Catal. A Gen.* **1999**, *188*, 229–240. [[CrossRef](#)]
38. Feng, J.; Xiong, W.; Ding, H.; He, B. Hydrogenolysis of glycerol over Pt/C catalyst in combination with alkali metal hydroxides. *Open Chem.* **2016**, *14*, 279–286. [[CrossRef](#)]
39. Raynal, F.; Etcheberry, A.; Cavaliere, S.; Noël, V.; Perez, H. Characterization of the instability of 4-mercaptoaniline capped platinum nanoparticles solution by combining LB technique and X-ray photoelectron spectroscopy. *Appl. Surf. Sci.* **2006**, *252*, 2422–2431. [[CrossRef](#)]

40. Spataru, T.; Osiceanu, P.; Marcu, M.; Lete, C.; Munteanu, C.; Spa, N. Functional effects of the deposition substrate on the electrochemical behavior of platinum particles. *Jpn. J. Appl. Phys.* **2012**, *51*, 090119. [[CrossRef](#)]
41. Marcus, P.; Hinnen, C. XPS study of the early stages of deposition of Ni, Cu and Pt on HOPG. *Surf. Sci.* **1997**, *392*, 134–142. [[CrossRef](#)]
42. Motin, A.M.; Haunold, T.; Bukhtiyarov, A.V.; Bera, A.; Rameshan, C.; Rupprechter, G. Surface science approach to Pt/carbon model catalysts: XPS, STM and microreactor studies. *Appl. Surf. Sci.* **2018**, *440*, 680–687. [[CrossRef](#)]



© 2018 by the authors. Licensee MDPI, Basel, Switzerland. This article is an open access article distributed under the terms and conditions of the Creative Commons Attribution (CC BY) license (<http://creativecommons.org/licenses/by/4.0/>).